Mechanical Systems and Signal Processing 93 (2017) 415–430

Contents lists available at ScienceDirect

Mechanical Systems and Signal Processing

journal homepage: www.elsevier.com/locate/ymssp

Chaotic dynamics of size dependent Timoshenko beams with functionally graded properties along their thickness

J. Awrejcewicz [a,b,*], A.V. Krysko [c,d], S.P. Pavlov [e], M.V. Zhigalov [e], V.A. Krysko [e]

[a] Department of Automation, Biomechanics and Mechatronics, Lodz University of Technology, 1/15 Stefanowskiego St., 90-924 Lodz, Poland
[b] Department of Vehicles, Warsaw University of Technology, 84 Narbutta St., 02-524 Warsaw, Poland
[c] Department of Applied Mathematics and Systems Analysis, Saratov State Technical University, 77 Politehnicheskaya, 410054 Saratov, Russian Federation
[d] Cybernetic Institute, National Research Tomsk Polytechnic University, 30 Lenin Avenue, 634050 Tomsk, Russian Federation
[e] Department of Mathematics and Modeling, Saratov State Technical University, 77 Politehnicheskaya, 410054 Saratov, Russian Federation

ARTICLE INFO

Article history:
Received 27 September 2016
Received in revised form 15 January 2017
Accepted 27 January 2017

Keywords:
Nonlinear Timoshenko beam
Modified couple stress theory
Nonlinear dynamics
Chaos
Wavelet
Fourier spectra
Lyapunov exponents

ABSTRACT

Chaotic dynamics of microbeams made of functionally graded materials (FGMs) is investigated in this paper based on the modified couple stress theory and von Kármán geometric nonlinearity. We assume that the beam properties are graded along the thickness direction. The influence of size-dependent and functionally graded coefficients on the vibration characteristics, scenarios of transition from regular to chaotic vibrations as well as a series of static problems with an emphasis put on the load-deflection behavior are studied. Our theoretical/numerical analysis is supported by methods of nonlinear dynamics and the qualitative theory of differential equations supplemented by Fourier and wavelet spectra, phase portraits, and Lyapunov exponents spectra estimated by different algorithms, including Wolf's, Rosenstein's, Kantz's, and neural networks. We have also detected and numerically validated a general scenario governing transition into chaotic vibrations, which follows the classical Ruelle-Takens-Newhouse scenario for the considered values of the size-dependent and grading parameters.

1. Introduction

A functionally graded material (FGM) can be made by mixing two or more materials with the required continuous properties along a defined direction [1]. Continuous changes in the material properties of the FGM yield a lot of engineering benefits, since this approach allows one to avoid an occurrence of large shear stresses, which are typically observed while fabricating multi-layer beams. It should be emphasized that the static bending as well as the dynamic characteristics of the structural members made from FGM have been intensively studied recently [2–10].

The mentioned materials can be applied in many scientific and engineering fields such as aerospace, automobile, electronics, optics, chemistry, biomedical engineering, nuclear engineering, mechanical engineering, and in manufacturing of elements of micro- and nano-electromechanical systems (MEMS/NEMS). FGM are widely used in micro- and nanostructures, including thin films/layers (see the works of Fu et al. [11,12]), and MEMS/NEMS (as shown in the works of Witvrouw et al.

* Corresponding author at: Department of Automation, Biomechanics and Mechatronics, Lodz University of Technology, 1/15 Stefanowskiego St., 90-924 Lodz, Poland.
E-mail addresses: awrejcew@p.lodz.pl (J. Awrejcewicz), anton.krysko@gmail.com (A.V. Krysko), pspsar@yandex.ru (S.P. Pavlov), zhigalovm@ya.ru (M.V. Zhigalov), tak@san.ru (V.A. Krysko).

http://dx.doi.org/10.1016/j.ymssp.2017.01.047
0888-3270/

[13] or Lee et al. [14]). What should be mentioned is that the thickness of beams employed in the above-mentioned applications is of an order of microns and submicrons, and thus the influence of the small scale effects on the behavior of such beams can be significant. Hence, it is of great importance to analyze the dynamics of such beams.

The experiments described in the works [15–17,28] show that small size effects play an important role in materials with a microscale structure, such as a thin copper wire, single crystal silver, nickel or steel epoxy polymeric beams. Namely, this phenomenon is exhibited when the characteristic dimension of the beam, i.e. either the beam thickness or size, is close to the internal material length scale parameter (as stated by Kong Shengli et al. in [18]).

The classical theory of elasticity does not enable one to predict and account for the small size effect that occurs in the micro- and submicro-scale structures. To explain these effects, various size-dependent continuum theories have been proposed, for example, the couple stress elasticity theory [19,20], nonlocal polar elastic continua theory (see the work by Eringen [21]), micropolar theory (described by Eringen in [22]), strain gradient elasticity and gradient plasticity (see the work by Aifantis [23]), and surface elasticity (described by Gurtin in [24]).

In the couple stress theory, two additional material constants can be distinguished (according to Toupin et al. [19] and Mindlin et al. [20]). For isotropic elastic materials, they are related to the underlying microstructure of the material and are inherently difficult to determine. Equations of the couple stress theory [19,20] were modified by Yang et al. and proposed in [25]. As a result of the modifications, new equilibrium equations have been obtained with only length scale parameter of the material. Such a model simplified the implementation of the modified couple stress theory.

In what follows, we apply the modified couple stress theory [18,26,30,7] to study the Euler-Bernoulli, Timoshenko, and higher-order beam theories.

In reference [31], the size-dependent behavior of microbeams made of FGM has been investigated by Asghari et al. using the modified couple stress theory for the linear Euler-Bernoulli model.

The Timoshenko beam model, contrarily to the Euler-Bernoulli model, allows one to take into account the shear deformation and is more accurate for relatively thick beams and beams of materials of low shear stiffness. The modified couple stress theory aimed at investigating the size-dependent behavior of the homogeneous Timoshenko beam has been studied in reference by Ma et al. [27]. In other work by Asghari et al. [32], these results have been extended for the Timoshenko beams made from FGM. Furthermore, a closed analytical formula has been obtained for the case of statics as well as the size-dependent frequencies have been detected and studied.

In reference [33], Arbind and Reddy investigated functionally graded beams with properties graduation along the thickness and the von Kármán nonlinear strains by means of employing the modified couple stress theory. The nonlinear PDEs governing the dynamics of both Euler-Bernoulli and Timoshenko beams have been analyzed. In addition, the effect of nonlinearity, shear deformation, power-law index, microstructural length scale, and boundary conditions on the bending response of beams under mechanical loads have been presented.

It should be mentioned that nonlinear equations governing the microstructural dependences in beams made from FGM have been derived in other work by Arbind et al. [34], where a general third-order beam theory as well as the Bernoulli–Euler and Timoshenko beam theories (as special cases) have been investigated.

Scheible et al. [29] have experimentally observed that the effects of nonlinearities on the behavior of micro- and nanomechanical resonators are very significant even if the amplitudes of the excitation are not large. Hence, studying the nonlinear/chaotic dynamics of such NEMS/MEMS devices is crucial for getting appropriate and accurate results while analyzing or designing such elements. It should be noted that when the chaotic dynamics of such beams is exhibited, the beams vibrations are large and cause numerous harmful effects on the studied structural systems. It means that in general, the design of the studied structural members should prevent the chaotic response of the system. Namely, having obtained a set of parameters associated with the occurrence of chaotic zones, one may avoid this harmful behavior. This stands for the motivation of our study aimed at an analysis of such harmful vibrations. In addition to the applied aspects of our analysis, novel theoretical results associated with a scenario of transition from regular to chaotic dynamics of the studied size-dependent Timoshenko beam are presented in the paper. However, the critical literature review implies that there is a lack of investigations of the chaotic dynamics of beams made from FGM and exhibiting, in particular, the size-dependent behavior.

Investigations of nonlinear statics and dynamics of beams, plates, and shells have been carried out by the authors of the present paper for many years. In particular, problems devoted to solutions of nonlinear/chaotic continuous dynamical systems [35–42] have been studied. Furthermore, the analysis of nonlinear dynamics of mechanical constructions has been conducted taking into account different types of the nonlinearity, including geometrical, physical, and fabrication ones, and including actions of various physical fields like thermal, electric, magnetic, and mechanical [43,44] as well as white-noise interaction [45].

The monograph by Awrejcewicz et al. [46] focuses on the computational analysis of nonlinear vibrations of structural members (beams, plates, panels, shells), where studying of dynamical problems can be reduced to considering one spatial variable and time. The simplification is introduced based on a formal mathematical approach aimed at reducing the problems with an infinite dimension to the problems of a finite one. The process includes also a transition from governing nonlinear partial differential equations to a set of a finite number of ordinary differential equations.

An important issue while investigating the nonlinear dynamics is the study of the largest Lyapunov exponent. In the literature, numerous methods to calculate the largest Lyapunov exponent are distinguished, e.g., Wolf's [54], Rosenstein's [55], Kantz's [56], Benettin's [57], Shimada and Nagashima's [58], Stefanski's [59], and other. The authors of the present paper have developed an approach based on neural networks [62]. The method allows one to calculate the whole spectrum of

Lyapunov exponents. Eventually, all the above-mentioned methods are used in this paper to calculate the largest Lyapunov exponent based on the analysis of the signal.

In the present paper, the chaotic dynamics of the size-dependent FG Timoshenko beams with the von Kármán nonlinearity is investigated for the first time based on the modified couple stress theory by Yang et al. [25]. We report the influence of the length scale parameter and the grading parameter on the vibration characteristics and supplement the investigations with a scenario of transition from regular to chaotic vibrations. As a result, it has been shown that beams modeled by the classical theory of continuum have less normalized deflection in comparison to the models yielded by the modified stress couple theory, independently of the material distribution along the beam thickness. It has been detected that the beam dynamics is most essentially influenced by the coefficient describing the heterogeneity of the material.

Finally, we have found that, for a set of fixed values of the parameters, including the size and material grading coefficients, regular vibrations of the beam tend to chaotic vibrations, following the Ruelle-Takens-Newhouse scenario.

2. Mathematical background

According to Yang et al. [25], in the modified couple stress theory, the strain energy U for a linear elastic body occupying the volume V has the form:

$$U = \frac{1}{2}\iiint_V \left(\sigma_{ij}\varepsilon_{ij} + m_{ij}\chi_{ij}\right) dV. \tag{1}$$

Now, for isotropic material, one can write

$$\sigma_{ij} = \lambda\varepsilon_{mm}\delta_{ij} + 2\mu\varepsilon_{ij}, \tag{2}$$

$$\varepsilon_{ij} = \frac{1}{2}\left(u_{i,j} + u_{j,i}\right), \tag{3}$$

$$m_{ij} = \beta\chi_{ij} = 2\mu l^2\chi_{ij}, \tag{4}$$

$$\chi_{ij} = \frac{1}{2}\left(\theta_{i,j} + \theta_{j,i}\right), \tag{5}$$

where σ_{ij}, ε_{ij}, m_{ij}, and χ_{ij} denote components of the following tensors: the Cauchy stress tensor $\boldsymbol{\sigma}$, the strain tensor $\boldsymbol{\varepsilon}$, the deviator part of the couple stress tensor $\mathbf{m}$, and the symmetric curvature tensor $\boldsymbol{\chi}$, respectively. In addition, u_i are components of the displacement vector, and $\mathbf{u}$, $\boldsymbol{\theta}$ stand for the infinitely small vector of rotation with components θ_i. Observe that $\theta_i = (rot(\mathbf{u}))_i/2$. Two Lamé constants are denoted by λ and μ, whereas l stands for the internal material length scale parameter.

Consider a beam of the length L and a rectangular cross section. The x-coordinate is taken along the length of the beam (it coincides with the reference line), z-coordinate along the thickness (the height) of the beam, and the y-coordinate along the width of the beam, as shown in Fig. 1. The coordinate z (Fig. 1) denotes a distance between the cross section points and the reference line.

$G(x,t)$ denotes a force acting on the axial cross section along the body axis OX per beam unit length. The parameter $C(x,t)$ presents the y component of the resultant volume moment per unit beam length. The resultant of the transverse stress acting on the upper side of the beam and the transverse volume forces per unit beam length is denoted by $q(x,t)$.

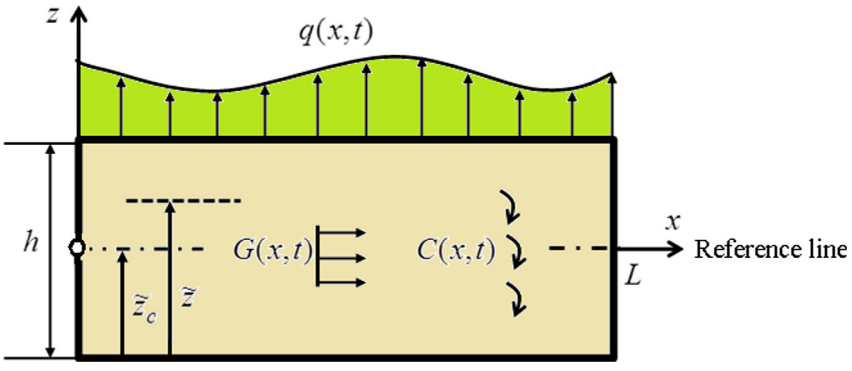

Fig. 1. Beam geometry and loading.

Coordinates z and $\tilde{z}$ (see Fig. 1) denote the distance between an arbitrarily chosen point and the reference line or the bottom surface, respectively. Also, the distance between the reference line and the bottom surface or the axial coordinate are represented by $\tilde{z}_c$ and x, respectively. It is assumed that the beam properties are constant along the axis OX.

For the beam made from FGM, the variation of properties along the thickness coordinate z is assumed to be represented as:

$$E(\tilde{z}) = E_0 + \frac{\tilde{z}+\frac{h}{2}}{h}(E_1 - E_0), \quad \mu(\tilde{z}) = \mu_0 + \frac{\tilde{z}+\frac{h}{2}}{h}(\mu_1 - \mu_0), \quad \rho(\tilde{z}) = \rho_0 + \frac{\tilde{z}+\frac{h}{2}}{h}(\rho_1 - \rho_0). \tag{6}$$

where $E_1(\tilde{z})$, $E_2(\tilde{z})$ - Young's modulus, $\mu_1(\tilde{z})$, $\mu_2(\tilde{z})$ - shear modulus, $\rho_1(\tilde{z})$, $\rho_2(\tilde{z})$ - density of the constituent materials of the functionally graded beam.The kinematic relations of the Timoshenko beam follow [47]:

$$u_x = u(x,t) + z\psi(x,t), \quad u_y = 0, \; u_z = w(x,t), \tag{7}$$

where $u(x,t)$, $w(x,t)$, and $\psi(x,t)$ denote the axial shift of the beam middle line, the transverse beam deviation, and the angle of rotation of the transverse beam cross section with respect to the vertical direction, respectively.

Using (7) as well as assuming very small slopes in the beam after deformation and a possible finite transverse deflection, the nonzero components of the strain tensor can be approximately expressed by the von Kármán relation [48]:

$$\varepsilon_{xx} = u_{,x} + \frac{1}{2}(w_{,x})^2 + z\psi_{,x}, \quad \varepsilon_{xz} = \frac{1}{2}(\psi + w_{,x}). \tag{8}$$

Furthermore, $\theta_i = (rot\,(\mathbf{u}))_i/2$ yields

$$\theta_y = \frac{1}{2}(\psi - w_{,x}), \quad \theta_x = 0. \tag{9}$$

Substituting (9) into (5), one obtains the following expression for a component of the symmetric part of the curvature tensor:

$$\chi_{xy} = \chi_{yx} = \frac{1}{4}(\psi_{,x} - w_{,xx}). \tag{10}$$

Assuming that the material properties change only with respect to the thickness, neglecting Poisson's effect as well as substituting (8) in (2), the following components of the stress tensor are obtained with respect to the kinematic parameters

$$\sigma_{xx} = E(\tilde{z})\left(u_{,x} + \frac{1}{2}(w_{,x})^2 + z\psi_{,x}\right), \quad \sigma_{xz} = k_s\mu(\tilde{z})(w_{,x} + \psi), \tag{11}$$

where $E(\tilde{z})$ and $\mu(\tilde{z})$ denote Young's modulus and shear modulus, respectively, and k_s stands for the correction coefficient, which is introduced due to the assumption of the graded shear strain regarding the beam transverse section, which depends on the form of the beam cross sections.

Substituting (10) into (4), one finds components of the deviator part of the tensor of the higher-order moments, which are expressed by the kinematic parameters:

$$m_{xy} = m_{yx} = \frac{1}{4}\beta(\tilde{z})(\psi_{,x} - w_{,xx}). \tag{12}$$

For further investigations, it is convenient to introduce a reference line for the z-coordinate, using the condition

$$B_{11} = \int_A E(\tilde{z})z dA = \int_A E(\tilde{z})(\tilde{z} - \tilde{z}_c)dA = 0 \tag{13}$$

From (13) one obtains the coordinate $\tilde{z}_c$ of the reference line

$$\tilde{z}_c = \frac{\int_A E(\tilde{z})\tilde{z}dA}{\int_A E(\tilde{z})dA}. \tag{14}$$

The expression (14) allows one to exclude the terms with coefficients B_{11} from the system of equations, what significantly simplifies the system of equations presented in references by Arbind et al. and Ke et al. [33,48].

3. Derivation of the equations of motion

In order to derive equations of motion of the FG Timoshenko beam using the modified couple stress theory, we substitute (8)–(12) in the expression for the strain energy U (1). As a result, the following strain energy U and kinetic energy K are obtained

$$\begin{aligned} U &= \frac{1}{2}\int_0^L \int_A \left(\sigma_{ij}\varepsilon_{ij} + m_{ij}\chi_{ij}\right) dA\, dx \\ &= \frac{1}{2}\int_0^L \int_A \left\{ E(\tilde{z})\left(u_{,x} + \frac{1}{2}(w_{,x})^2 + z\psi_{,x}\right)^2 + k_s\mu(\tilde{z})(\psi + w_{,x})^2 + \frac{1}{8}\beta(\tilde{z})(\psi_{,x} - w_{,xx})^2 \right\} dA\, dx\,, \end{aligned} \tag{15}$$

$$K=\frac{1}{2}\int_0^L\int_A \rho(\tilde{z})\left\{(u_{,t}+z\psi_{,t})^2+(w_{,t})^2\right\}dAdx, \tag{16}$$

where L stands for the beam length.

Variation of the work δW generated by the external forces, the distributed moments, and stresses on a threshold surface take the form

$$\delta W=\int_0^L\left(G\delta u+q\,\delta w+c\delta\theta_y\right)dx+\left(\overline{N}\delta u+\overline{V}\delta w+\overline{M}_\sigma\delta\psi+\overline{M}_m\delta\theta_y\right)\Big|_{x=0}^{x=L}, \tag{17}$$

where the external forces acting on the beam ends in the axial direction, the external transverse forces, the external bending moment generated by the normal stress σ_{xx}, and the external bending moment caused by the moment m_{xy} are denoted by $\overline{N}$, $\overline{V}$, $\overline{M}_\sigma$ and $\overline{M}_m$, respectively.

Owing to (13), relations (15) and (16) take the following form

$$U=\frac{1}{2}\int_0^L\left\{k_1\left(u_{,x}+\frac{1}{2}(w_{,x})^2\right)^2+k_2(\psi_{,x})^2+k_3(\psi+w_{,x})^2+k_4\left(\psi_{,x}-w_{,xx}\right)^2\right\}dx\,, \tag{18}$$

$$K=\frac{1}{2}\int_0^L\left\{m_0(u_{,t})^2+2Q\,u_{,t}\psi_{,t}+\tilde{I}(\psi_{,t})^2+m_0(w_{,t})^2\right\}dx. \tag{19}$$

where

$$\begin{aligned}
&k_1=\textstyle\int_A E(\tilde{z})\,dA,\ k_2=\int_A E(\tilde{z})z^2\,dA=\int_A E(\tilde{z})\,(\tilde{z}-\tilde{z}_c)^2dA,\\
&k_3=k_s\textstyle\int_A\mu(\tilde{z})\,dA,\ k_4=\frac{1}{8}\int_A\beta(\tilde{z})\,dA=\frac{1}{4}\int_A\mu(\tilde{z})l^2(\tilde{z})\,dA,\\
&m_0=\textstyle\int_A\rho(\tilde{z})\,dA,\ Q=\int_A\rho(\tilde{z})z\,dA=\int_A\rho(\tilde{z})\,(\tilde{z}-\tilde{z}_c)dA,\\
&\tilde{I}=\textstyle\int_A\rho(\tilde{z})z^2\,dA=\int_A\rho(\tilde{z})\,(\tilde{z}-\tilde{z}_c)^2dA\,.
\end{aligned} \tag{20}$$

Hamilton's principle yields

$$\delta\int_{t_1}^{t_2}(K-U+W)\,dt=0. \tag{21}$$

The carried-out variation with respect to u, w and ψ, integration by parts, and setting the terms standing by δu, δw and $\delta\psi$ to be equal to zero yield the following equations of motion

$$\begin{aligned}
&\left[k_1(u_{,x}+\frac{1}{2}(w_{,x})^2)\right]_{,x}+G=m_0u_{,tt}+Q\,\psi_{,tt}\\
&\left[k_2\psi_{,x}+k_4\left(\psi_{,x}-w_{,xx}\right)\right]_{,x}-k_3(\psi+w_{,x})+\frac{C}{2}=Q\,u_{,tt}+\tilde{I}\psi_{,tt},\\
&\left\{\left[k_1(u_{,x}+\frac{1}{2}(w_{,x})^2)\right]w_{,x}+\ k_3(\psi+w_{,x})\right\}_{,x}+\left[k_4(\psi_{,x}-w_{,xx})\right]_{,xx}+q+\frac{C_{,x}}{2}=m_0w_{tt},
\end{aligned} \tag{22}$$

the following boundary conditions

$$\left[k_1(u_{,x}+\frac{1}{2}(w_{,x})^2)-\overline{N}\right]\Big|_{x=0,L}=0$$

or $\delta u|_{x=0,L}=0$,

$$\left[k_2\psi_{,x}+k_4\left(\psi_{,x}-w_{,xx}\right)-\overline{M}_\sigma-\frac{\overline{M}_m}{2}\right]\Big|_{x=0,L}=0 \tag{23}$$

or $\delta\psi|_{x=0,L}=0$,

$$\left\{\left[k_1(u_{,x}+\frac{1}{2}(w_{,x})^2)\right]w_{,x}+\ k_3(\psi+w_{,x})+k_4\left(\psi_{,xx}-w_{,xxx}\right)+\frac{C}{2}-\overline{V}\right\}\Big|_{x=0,L}=0$$

or $\delta w|_{x=0,L}=0$,

$$\left(k_4(\psi_{,x}-w_{,xx})+\frac{\overline{M}_m}{2}\right)\Big|_{x=0,L}=0 \text{ or } \delta w_{,x}\big|_{x=0,L}=0\,,$$

and the initial conditions

$$\begin{aligned} &w(x,0)=\varphi_1(x), \quad w(x,0)_{,t}=\varphi_2(x),\\ &u(x,0)=\varphi_3(x), \quad u(x,0)_{,t}=\varphi_4(x),\\ &\psi(x,0)=\varphi_5(x), \quad \psi(x,0)_{,t}=\varphi_6(x). \end{aligned} \tag{24}$$

The equations of motion (22) of the nonlinear Timoshenko beam made from FGM and the boundary conditions (23) are obtained using the relation (14).

4. Statement of the problem

For further numerical investigations, to simplify the problem, the following parameters are fixed: $G(x,t)=0$, $(x,t)=0$. To construct the rules of the change of the beam characteristics along the beam thickness, parameters including Young's modulus $E(\tilde{z})$, shear modulus $\mu(\tilde{z})$, and beam density $\rho(\tilde{z})$ are used.

The considered FGM microbeams consist of Titan (Ti) and Nickel (Ni) with the material properties $E_0=105$ GPa, $\rho=4940$ kg/m^2, $\nu=0.31$ for Ti and $E_1=210$ GPa, $\rho=8902$ kg/m^2, $\nu=0.3$ for Ni.

The required integration is carried out in formulas (14) and (20) by using the following coupling between the elastic and shear moduli

$$E_1=P_E E_0,\ \mu_1=P_\mu\mu_0, \rho_1=P_\rho\rho_0. \tag{25}$$

Substituting (6) and (25) in (14), one obtains:

$$\tilde{z}_c=\frac{h}{12}\frac{P_E-1}{1+\frac{1}{2}(P_E-1)}. \tag{26}$$

Formula (26) implies that for $P_E>1$, $(\tilde{z}_c>0)$ and the neutral line is shifted above in comparison to the neutral line of the homogeneous beam $(P_E=1)$. In the case $P_E<1$, $\tilde{z}_c<0$, and the neutral line is shifted below the neutral line of the counterpart homogeneous beam.

Using (6), (25) and (26), and taking into account (20), the following coefficients are defined

$$\begin{aligned} &k_1=E_0A\left[1+\tfrac{1}{2}(P_E-1)\right],\ k_2=\tfrac{1}{12}E_0Ah^2\left[\tfrac{3}{2}+\frac{(P_E-1)^2}{12\left(1+\frac{1}{2}(P_E-1)\right)}\right],\\ &k_3=k_s\mu_0A\left[1+\tfrac{1}{2}(P_\mu-1)\right],\ k_4=\tfrac{1}{4}\mu_0Al^2\left[1+\tfrac{1}{2}(P_\mu-1)\right],\\ &m_0=\rho_0A\left[1+\tfrac{1}{2}(P_\mu-1)\right],\ Q=\rho_0A\tfrac{h}{12}\left[(P_\rho-1)-\tfrac{1}{2}\frac{(P_E-1)(P_\rho+1)}{1+\frac{1}{2}(P_E-1)}\right],\\ &\tilde{I}=\rho_0A\tfrac{h^2}{12}\left[\left(1+\frac{(P_E-1)^2}{12\left(1+\frac{1}{2}(P_E-1)\right)^2}\right)\left(1+\tfrac{1}{2}(P_\rho-1)\right)-\tfrac{1}{6}\frac{(P_E-1)(P_\rho+1)}{1+\frac{1}{2}(P_E-1)}\right]. \end{aligned} \tag{27}$$

The shear coefficient k_s is taken as $5/6$, which is most suitable for the description of the behavior of beams with rectangular cross sections, as described by Ke et al. in [48]. In what follows, we introduce the following dimensionless parameters:

$$\begin{aligned} &\bar{w}=\tfrac{w}{h},\ \bar{u}=\tfrac{ua}{h^2},\ \bar{\psi}=\tfrac{\psi a}{h},\ \bar{x}=\tfrac{x}{a},\ \gamma_1=\tfrac{a}{h},\ \gamma_2=\tfrac{l}{h},\ \bar{q}=q\tfrac{a^2}{h^2E},\\ &\bar{t}=\tfrac{t}{\tau},\ \tau=\tfrac{a}{c},\ c=\sqrt{\tfrac{E}{\rho}},\ \bar{\varepsilon}=\varepsilon\tfrac{a}{c},\ \bar{k}_1=\tfrac{k_1}{AE_0},\ \bar{k}_2=\tfrac{k_2}{AE_0h^2},\ \bar{k}_3=\tfrac{k_3}{AE_0},\ \bar{k}_4=\tfrac{k_4}{AE_0l^2}. \end{aligned} \tag{28}$$

Taking into account the introduced simplifications and notation as well as omitting the bars over dimensionless parameters, the following dimensionless beam equations are eventually obtained:

$$\begin{aligned} &k_1\left[u_{,x}+\frac{1}{2}(w_{,x})^2\right]_{,x}=u_{,tt}\\ &k_2\psi_{,xx}+3k_4\gamma_2^2\left(\psi_{,xx}-w_{,xxx}\right)-12k_sk_3\gamma_1^2(\psi+w_{,x})==\psi_{,tt}\ ,\\ &\frac{1}{\gamma_1^2}\left\{k_1\left[(u_{,x}+\frac{1}{2}(w_{,x})^2)\right]w_{,x}\right\}_{,x}+k_3\left(\psi_{,x}+w_{,xx}\right)+k_4\frac{\gamma_2^2}{\gamma_1^2}\left(\psi_{,xxx}-w_{,xxxx}\right)+q=w_{,tt}+\varepsilon w_{,t} \end{aligned} \tag{29}$$

Hereafter, all the considerations are made for the dimensionless form.

We restrict further considerations to the following boundary conditions (rigid clamping of the beam ends):

$$\begin{aligned} w(0,t) &= w(1,t) = 0, \quad w_{,x}(0,t) = w_{,x}(1,t) = 0, \\ u(0,t) &= u(1,t) = 0, \quad \psi(0,t) = \psi(1,t) = 0, \end{aligned} \tag{30}$$

and the following initial conditions:

$$w(x,0) = w_{,t}(x,0), \quad u(x,0) = u_{,t}(x,0) = 0, \quad \psi(x,0) = \psi_{,t}(x,0) = 0. \tag{31}$$

Reduction of the PDEs (29)–(31) is carried out by means the finite difference method (FDM) of the second-order accuracy, and the finite element method (FEM). Both FDM and FEM were used to validate the results.

We have compared numerical results yielded by the 4th and 6th order Runge-Kutta methods. Owing to the coincidence of results and the study by Krysko et al. in [49], we have further employed the 4th order Runge-Kutta method. The optimal number of the spatial mesh elements regarding the beam length has been chosen on the basis of the Runge principle.

5. Results and discussions

Numerical investigations of static and dynamic problems have been reported for the following fixed system parameters: relative beam length $\gamma_1 = \frac{a}{h} = 30$, size-dependent parameter $\gamma_2 = \frac{l}{h} = 0;\ 0.3$. Young's and shear coefficients regarding the thickness (25) are taken as $P_E = P_\mu = P_\rho = P = 1;\ 2;\ 0.5$. This choice fits with the formulas for the coefficients given by (27). All numerical results are within the applicability of the introduced hypotheses.

5.1. Reliability and validity of the obtained results

To check the reliability of the results obtained for the Timoshenko beam model, solutions obtained with the use of FDM and FEM are compared. Then, the problem is studied for clamping-clamping boundary conditions and for the zero initial condition. The curves of the dependence of the maximum deflection on the amplitude of the external load, obtained with different computational methods (see Fig. 2), fully coincide in the case of regular beam vibrations, whereas slight differences appear for chaotic dynamics (Fig. 2).

On the basis of results presented in Fig. 2, one can conclude that values of $w_{\max}$ fully coincide for both applied computational approaches if the excitation amplitude corresponds to regular vibrations. Small differences are noticeable in the case of chaotic dynamics. Vibration scales obtained by the two methods fully coincide. For FDM, the transition to chaos appears later than for FEM and the chaotic regime is smaller if the FDM approach is applied.

5.2. Problems of statics

We solve the problems of statics by using equations governing the dynamics (29)–(31). This method will be further referred to as the relaxation method (see the work by Awrejcewicz et al. [46]).

If the load $[\bar{q}]$ does not depend on time, a static solution to the problem can be yielded by the dynamic approach. Namely, the initial condition plays a role of an excitation, whereas the term with the first time derivative, including the dissipation/-damping coefficient, presents a dissipative character of the excited solution. A solution to the so far defined dynamic problem can be found through the employment of an arbitrary method aimed at solving the Cauchy problem. Once a stationary state is achieved, the counterpart static problem is solved.

The above-mentioned idea of finding solutions to stationary problems as parts of nonstationary problems for increasing time has been first illustrated by A.N. Tichonov. The applied relaxation technique can be derived as the iterational method to solve linear and nonlinear problems of the algebraic and transcendential equations, where a step in time defines a new approximation for an unknown root of an equation. One more benefit of the relaxation method includes the simplicity of its computer implementation, since there exists a wide palette of effective algorithms aimed at solving the Cauchy problem [50–53].

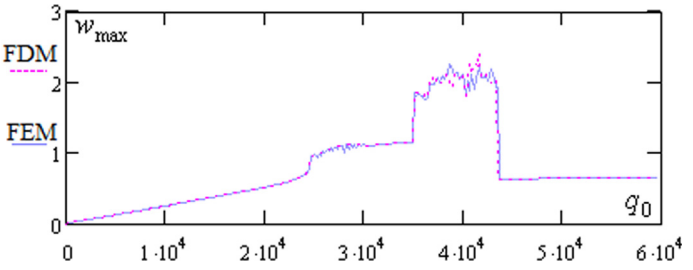

Fig. 2. Maximum deflection as a function of the excitation amplitude.

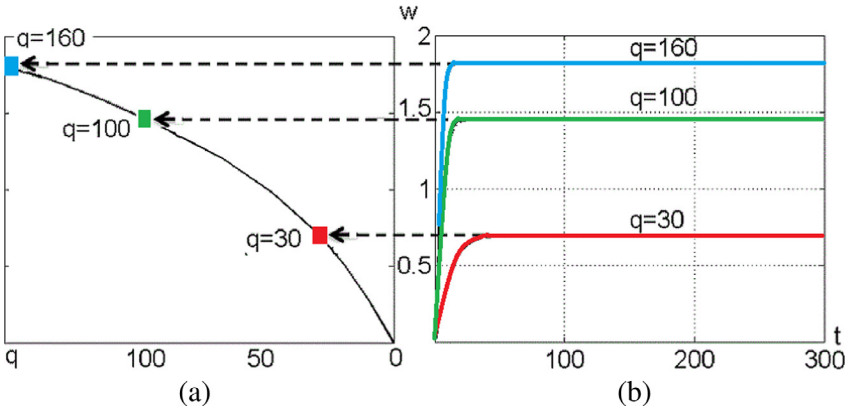

Fig. 3. The load–deflection (a) and the deflection–time dependences (b).

Table 1
The values of the γ_2, P_E parameters in the studied cases.

Case number	1	2	3	4	5	6	7	8
Parameters	$\gamma_2 = 0.3$ $P_E = 1$	$\gamma_2 = 0.3$ $P_E = 0.5$	$\gamma_2 = 0.3$ $P_E = 2$	$\gamma_2 = 0$ $P_E = 1$	$\gamma_2 = 0$ $P_E = 0.5$	$\gamma_2 = 0$ $P_E = 2$	$\gamma_2 = 0$ $P_E = 1$ $E = 2E_0$	$\gamma_2 = 0.3$ $P_E = 1$ $E = 2E_0$

The results of solving the static problem for $\gamma_2 = l/h = 0.3$ and $\varepsilon = 3$ are reported in Fig. 3. In Fig. 3a the load–deflection dependence yielded by the relaxation method is shown for the given values of $q(x) = q = const$. In Fig. 3b, the stationary part of the dynamical process of the beam deflection $w(t)$ is reported for $q = 30, 100, 160$.

The $w(t)$ histories show that the steady/static state is achieved relatively fast for the fixed dissipation coefficient for all loads. For the load amplitude $q = 30$, the steady state is achieved at $t = 49$, whereas for $q = 100, 160$, at $t = 28$ and $t = 19$, respectively. Therefore, the employed method is highly stable and allows one to solve nonlinear static problems without any numerical difficulties.

The results of application of the relaxation method to study eight different combinations of the size-dependent parameter γ_2 and the material grading parameter P_E (the damping coefficient $\varepsilon = 3$) are shown in Table 1.

The choice of parameters is as follows: $P = 1$ – homogeneous material; $P = 2$ – material with $E_1 = 2E$ on the upper side of the beam, and a material with $E_2 = E$ on the bottom side of the beam; $P = 0.5$ – reverse material arrangement ($2E$ on the bottom side). The results of the carried-out investigations are given in Fig. 4.

The analysis of $w(q)$ for $\gamma_2 = 0.3$ (Fig. 4a) shows that, for the same load ($q > 100$), the minimum value of the deflection is observed for the nonhomogeneous beam with the reinforcement (i.e. stiffer layer) on the upper side. The minimum value of the deflection is observed for the functionally graded beam in which the stiffer layer is located on the bottom side. If classical beams, i.e. those without the size-dependent factor, are considered (Fig. 4b), the distribution is similar. The investigation of the results obtained for homogeneous beams with different values of stiffness and the size-dependent coefficient (Fig. 4c) shows that the minimum deflection corresponds to the variant with the doubled stiffness and the size-dependent behavior of the material ($\gamma_2 = 0.3, P_E = 1, E = 2E_0$). A comparison of the results obtained for the same values of P (Fig. 4d) implies that the size-dependent behavior results in a decrease of the deflection values.

Observe that for the case 2, the deflection curve changes its position, i.e. for $q = 50$ it is located below the deflection of the case 6, for $q = 100$ it overlaps with the latter one, whereas for $q = 150$, it is above the afore-mentioned deflection.

In general, the size-dependent behavior reduces the deflection value for the same grading parameter. Placing the stiffer layer on the upper side of the beam essentially influences the deflection value for the same value of the size-dependent coefficient.

5.3. Dynamic problems

The investigation of dynamic problems consists of the determination of the eigenfrequencies of the linear counterpart problem and the investigation of the chaotic dynamics with respect to different combination of the parameters γ_2 and P.

5.3.1. Determination of the Timoshenko beam eigenfrequencies

In order to get the eigenfrequencies, we study the linear equations governing the size-dependent behavior in the functionally graded beams, which are yielded by system (30) if nonlinear terms are neglected. The following linear PDEs are obtained regarding the functions ψ, w:

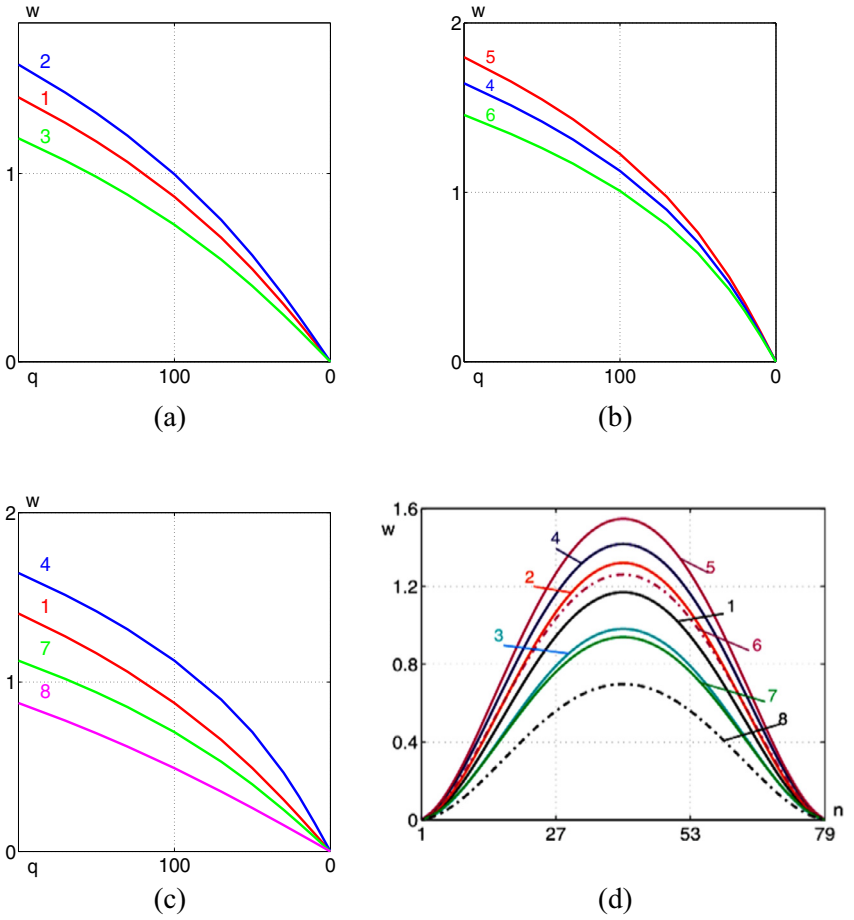

Fig. 4. Comparison of static solutions of the Timoshenko beam: (a) $w(q)$ for the cases 1–3, $\gamma_2 = 0.3$; (b) $w(q)$ for the cases 4–6, $\gamma_2 = 0$; (c) $w(q)$ for the homogeneous beam; (d) $w(n)$ for $q = 150$.

Table 2
The frequencies associated with the studied cases.

Case number	1	2	3	4	5	6	7	8
ω_0	4.9	4.5	5.4	3.9	3.7	4.05	5.9	6.7

$$\begin{aligned} &k_2\psi_{,xx} + 3k_4\gamma_2^2(\psi_{,xx} - w_{,xxx}) - 12k_sk_3\gamma_1^2(\psi + w_{,x}) = \psi_{,tt}\ , \\ &k_3(\psi_{,x} + w_{,xx}) + k_4\tfrac{\gamma_2^2}{\gamma_1^2}(\psi_{,xxx} - w_{,xxxx}) - q = w_{,tt}\,. \end{aligned} \tag{32}$$

Equations (32) are solved using the algorithm presented earlier. Table 2 reports the results obtained numerically, and the studied cases correspond to those shown in Table 1.

The carried-out analysis yields the following conclusions. The smallest eigenfrequency is exhibited by the FG beam when the stiffer material is located on the beam bottom side (this is case 5 without the size-dependent behavior). The largest eigenfrequency corresponds to the case 8, i.e. the size-dependent behavior is taken into account and the stiffness of the homogeneous beam is doubled. The size-dependent behavior strongly reduces the value of the eigenfrequency. For the homogeneous beam (cases 1, 4 and 7, 8), the change in the frequency value is of 10% and 12%, respectively. For FG beam (cases 2, 5 and 3, 6) – 18% and 25%, respectively. Therefore, the graded distribution of the beam thickness has an impact on the eigenfrequency value.

5.3.2. Investigation of the Timoshenko beam chaotic dynamics versus the combination of parameters γ_2 and P

The investigation of the solutions to the dynamic problems, i.e. when the excitation $q = q_0\sin(\omega_p t)$ is taken into account, has been carried out for the size-dependent coefficient $\gamma_2 = 0;\ 0.3$ and different values of P_E reported in Table 1.

The loading parameters are: $q_0 = 17000,\ \omega_p = 8$. The frequency $\omega_p = 8$ is essentially higher comparing to the arbitrary eigenfrequency given in Table 2. All obtained results are shown in Tables 3–10:

Table 3
$\gamma_2 = 0.3$, $P = 1$.

Time history	FFT	2D wavelet	Phase portrait	Poincaré section	LLE
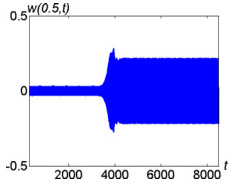	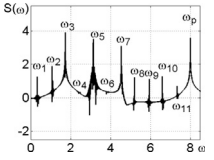	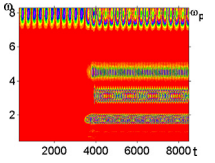	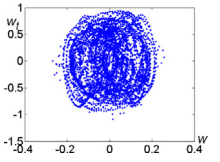	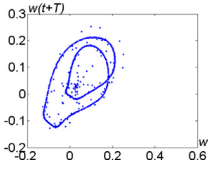	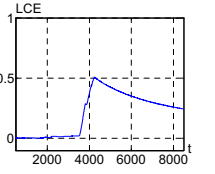

Table 4
$\gamma_2 = 0.3$, $P = 2$.

Time history	FFT	2D wavelet	Phase portrait	Poincaré section	LLE
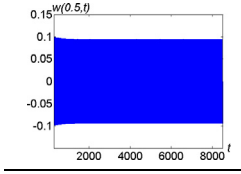	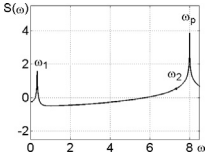	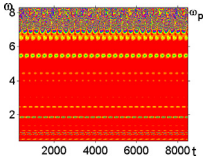	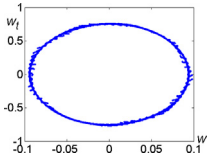	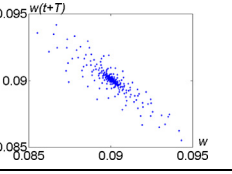	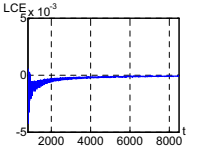

Table 5
$\gamma_2 = 0.3$, $P = 0.5$.

Time history	FFT	2D wavelet	Phase portrait	Poincaré section	LLE
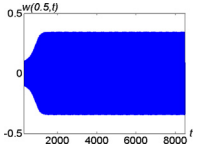	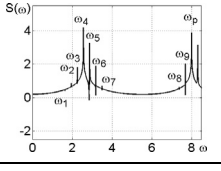	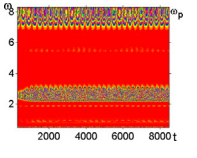	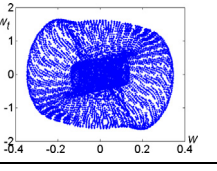	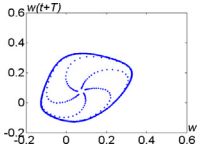	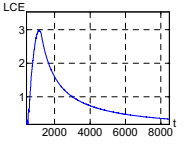

Table 6
$\gamma_2 = 0$, $P = 1$.

Time history	FFT	2D wavelet	Phase portrait	Poincaré section	LLE
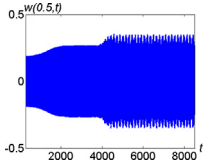	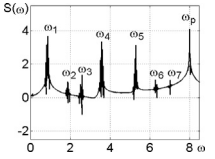	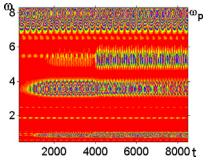	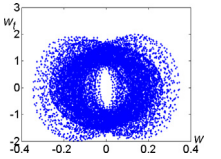	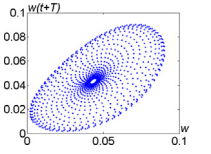	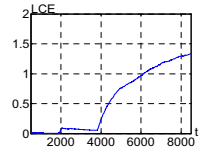

Table 7
$\gamma_2 = 0$, $P = 2$.

Time history	FFT	2D wavelet	Phase portrait	Poincaré section	LLE
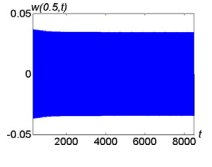	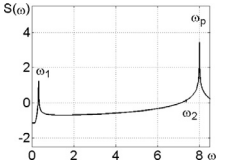	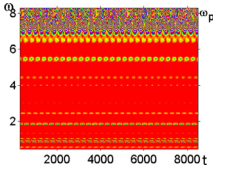	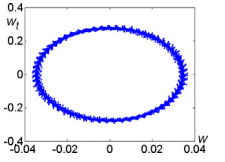	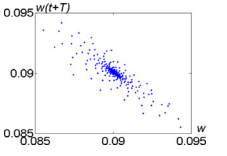	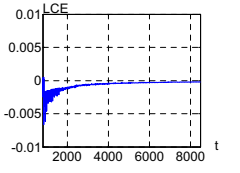

Table 8
$\gamma_2 = 0$, $P = 0.5$.

Time history	FFT	2D wavelet	Phase portrait	Poincaré section	LLE
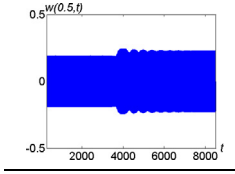	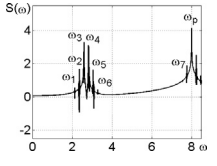	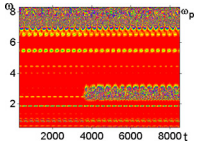	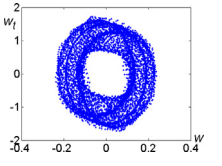	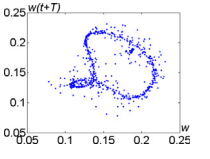	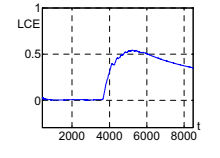

Table 9
$\gamma_2 = 0$, $P = 1$, $E = 2E_0$.

Time history	FFT	2D wavelet	Phase portrait	Poincaré section	LLE
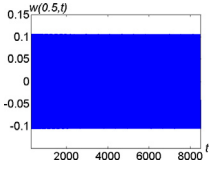	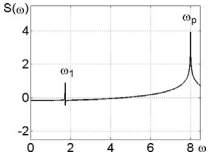	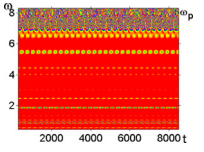	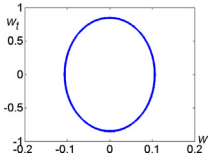	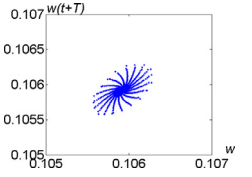	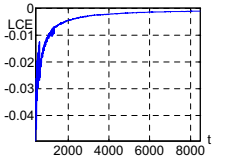

Table 10
$\gamma_2 = 0.3$, $P = 1$, $E = 2E_0$.

Time history	FFT	2D wavelet	Phase portrait	Poincaré section	LLE
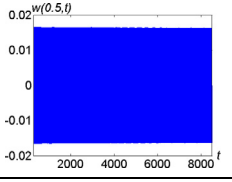	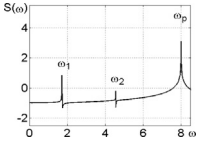	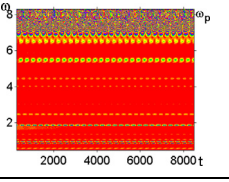	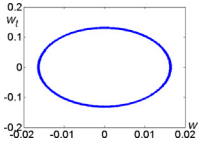	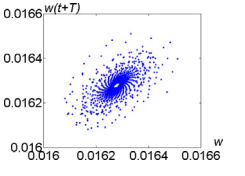	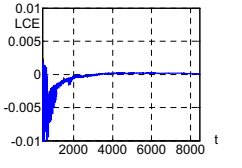

Table 3 ($\gamma_2 = 0.3$, $P = 1$, $E = E_0$) – homogeneous beam with the size-dependent behavior and an initial stiffness;
Table 4 ($\gamma_2 = 0.3$, $P = 2$) – functionally graded beam with the size-dependent behavior for the case when the stiffer layer is located on the upper side of the beam;
Table 5 ($\gamma_2 = 0.3$, $P = 0.5$) - functionally graded beam with the size-dependent behavior for the case when the stiffer layer is located on the bottom side of the beam;
Table 6 ($\gamma_2 = 0$, $P = 1$, $E = E_0$) – homogeneous beam without the size-dependent behavior and with an initial stiffness;
Table 7 ($\gamma_2 = 0$, $P = 2$) – nonhomogeneous beam without the size-dependent behavior for the case when the stiffer layer is located on the upper side of the beam;
Table 8 ($\gamma_2 = 0$, $P = 0.5$) – nonhomogeneous beam without the size-dependent behavior for the case when the stiffer layer is located on the bottom side of the beam;
Table 9 ($\gamma_2 = 0$, $P = 1$, $E = 2E_0$) – homogeneous beam without the size-dependent behavior and with a doubled stiffness;
Table 10 ($\gamma_2 = 0.3$, $P = 1$, $E = 2E_0$) – homogeneous beam with the size-dependent behavior and a doubled stiffness.

The following results are reported in the above-listed tables: (a) time history $w(0.5;t)$; (b) Fourier spectrum based on the Fast Fourier Transform (FFT) $S(\omega)$; (c) 2D wavelet spectrum based on the Morlet wavelet; (d) Poincaré section $w(t+T)[w(t)]$; (e) phase portrait $\dot{w}[w(t)]$; f) time evolution of the largest Lyapunov exponent (LLE) based on Wolf's algorithm [54].

The results obtained for the functionally graded beam with the location of the stiffer layer on the upper side (Table 4) essentially differ from the results shown in Tables 3 and 5. This beam exhibits quasi-periodic vibrations at three linearly dependent frequencies and the LLE is negative. Results reported in Tables 3 and 5 imply that the homogeneous beam and the functionally graded beam with the stiffer layer located on the bottom side vibrate chaotically. The difference between the results reported in Tables 3 and 5 is as follows. In the case of the homogeneous beam (Table 3), the transition into chaos takes place at $t = 3800$, which has been also validated by the wavelet spectrum and the LLE. On the contrary, the functionally graded beam (Table 5) starts to chaotically vibrate in the beginning of the time interval.

Therefore, the functionally graded beam with the stiffer layer located on the upper side can be employed for a given amplitude and frequency of the excitation load.

The analysis of the obtained results for the variants corresponding to a lack of the size-dependent behavior ($\gamma_2 = 0$) validates a conclusion that the beam with the stiffer layer located on the upper side can be employed to carry the dynamic load. It should be mentioned that all characteristics of the vibration process, i.e. Fourier and wavelet spectra, Poincaré section, and the LLEs qualitatively coincide. The carried-out analysis and comparison with the previous variants ($\gamma_2 = 0.3$) for the homogeneous beam and the beam with the stiffer layer located on the bottom side implies the essential difference in all characteristics of the vibrational process. In other words, for the studied structures, the size-dependent behavior plays an essential role.

The analysis of the results associated with the homogeneous beams (Tables 3 and 6–8) allows one to extend the conclusions formulated with respect to static problems. Namely, application of the material of large stiffness has an essential influence on the character of vibrations.

In the case of the beams with a single (initial) stiffness, chaotic vibrations occur (Tables 3 and 6), whereas in the case of beams with a doubled stiffness (Tables 7 and 8), quasi-periodic vibrations are exhibited.

In order to validate the reliability of the LLEs computation using Wolf's algorithm [54], we have computed them using three other methods, i.e. Rosenstein's [55], Kantz's [56], and neural network (NW) (proposed by the authors of the present paper) [62] approaches. The investigations have been carried out for all mentioned variants. In what follows, we give exemplary results regarding the case 1 (see Table 3). The numbers of time intervals correspond to the following values: 1 - $t \in [300; 2100]$, 2 - $t \in [2105; 2160]$, 3 - $t \in [2165; 3900]$, 4 - $t \in [3901; 5000]$, 5 - $t \in [5001; 8000]$.

All four methods yield positive values of the LLEs (λ_1) on all time intervals, which implies chaotic vibrations. However, there are some differences with respect to the computed values. The qualitative changes of λ_1 are similar for three methods (Wolf's, Rosenstein's, Kantz's) on the intervals 1–3. Beginning from the 3rd time interval, all three characteristics (Rosenstein's, Kantz's, neural networks (NW)) shown in Fig. 5 approach each other, and hence essentially differ from the values obtained using Wolf's method.

Fig. 6 reports time evolutions of the Lyapunov spectrum obtained with the neural network approach. One may observe the qualitative similarity between the curves corresponding to the first four Lyapunov exponents.

5.4. Scenarios of transition into chaos

One of essential aspects while investigating the dynamics of continuous mechanical systems comprises the detection and analysis of the scenario of transition from regular to chaotic dynamics. Scenarios of such transitions for classical beams, plates, and shells, including the Bernoulli-Euler and Timoshenko theories, have been described in Refs. [60–62]. In this work, we were aimed at analysing the scenario associated with the Timoshenko model, taking into account two cases, i.e. the one concerning the size-dependent behavior $\gamma_2 = 0.3$ and the through-thickness functionally graded beam for $P = 2$ or $P = 0.5$ as well as the one without the size-dependent effect ($\gamma_2 = 0$) and for the homogeneous beam $P = 1$ for $E = E_0,\ E = 2E_0$. The following parameters are fixed: $\omega_p = 8,\ \varepsilon = 1,\ \gamma_1 = 30,\ \nu = 0.3$.

On the basis of the obtained results, one may conclude that the scenarios of transition from regular to chaotic vibrations of the Timoshenko beam follow the classical Ruelle-Takens-Newhouse scenario for the all considered cases.

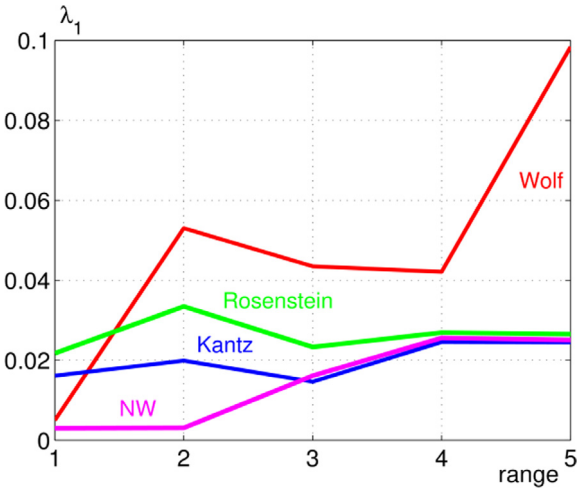

Fig. 5. Comparison of the LLE computed with four different algorithms.

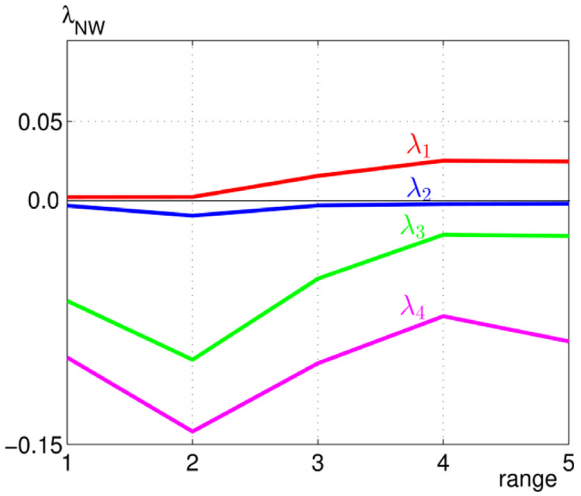

Fig. 6. Spectrum of the first four Lyapunov exponent obtained using the neural network method.

6. Concluding remarks

1. We have considered the dynamics of nonlinear FG Timoshenko beams based on the modified couple stress theory, using a novel concept of the reference line.
2. The influence of the size-dependent coefficient and the grading parameter on the load-deflection dependence is investigated for the static problem. In order to get solutions to nonlinear static problem, the relaxation method was employed. It has been shown that the minimum deflection is achieved by the beam when the functional grading process is taken into account and the stiffer layer is located on the upper side in both cases, i.e. with/without the size-dependent behavior.
3. The functionally graded beam with the stiffer layer on the upper side is suitable to carry dynamic loads at a given frequency and amplitude of the harmonic excitation. This conclusion coincides with that formulated for static problems. In the case of the homogeneous beam and the beam with the stiffer layer located on the bottom side, the essential dependence of the obtained results on the size-dependent coefficient is observed.
4. In order to validate the reliability of the LLEs computed with Wolf's algorithm, three qualitatively different methods have been employed, i.e. Rosenstein's, Kantz's, and the one based on neural network. The carried-out analysis implies that all methods give qualitatively the same result, i.e. positive or negative values of the LLEs, on the whole studied time interval.
5. For the considered values of the size-dependent and material grading parameters, the universal route to chaos, following the classical Ruelle-Takens-Newhouse scenario, has been detected.

Acknowledgement

This work has been supported by the Grant RSF No. 16-11-10138.

References

[1] M. Koizumi, The concept of FGM, Ceram. Trans. Funct. Grad Mater. 34 (1993) 3–10.
[2] B.V. Sankar, An elasticity solution for functionally graded beams, Comp. Sci. Tech. 61 (2001) 689–696.
[3] A. Chakraborty, S. Gopalakrishnan, J.N. Reddy, A new beam finite element for the analysis of functionally graded materials, Int. J. Mech. Sci. 45 (2003) 519–539.
[4] M. Aydogdu, V. Taskin, Free vibration analysis of functionally graded beams with simply supported edges, Mater. Des. 28 (2007) 1651–1656.
[5] Z. Zhong, T. Yu, Analytical solution of a cantilever functionally graded beam, Comp. Sci. Tech. 67 (2007) 481–488.
[6] J. Ying, C.F. Li, W.Q. Chen, Two-dimensional elasticity solutions for functionally graded beams resting on elastic foundations, Compos. Struct. 84 (2008) 209–219.
[7] X.F. Li, A unified approach for analyzing static and dynamic behaviors of functionally graded Timoshenko and Euler-Bernoulli beams, J. Sound Vib. 318 (2008) 1210–1229.
[8] H.J. Xiang, J. Yang, Free and forced vibration of a laminated FGM Timoshenko beam of variable thickness under heat conduction, Compos. Part B: Eng. 39 (2008) 292–303.
[9] R. Kadoli, K. Akhtar, N. Ganesan, Static analysis of functionally graded beams using higher order shear deformation theory, Appl. Math. Modell. 32 (2008) 2509–2525.
[10] M.A. Benatta, I. Mechab, A. Tounsi, E.A. Adda, Bedia, Static analysis of functionally graded short beams including warping and shear deformation effects, Comput. Mater. Sci. 44 (2008) 765–773.
[11] Y.Q. Fu, H.J. Du, S. Zhang, Functionally graded TiN/TiNi shape memory alloy films, Mater. Lett. 57 (20) (2003) 2995–2999.
[12] Y.Q. Fu, H.J. Du, W.M. Huang, S. Zhang, M. Hu, TiNi-based thin films in MEMS applications: a review, Sensors Actuat. A 112 (2–3) (2004) 395–408.
[13] A. Witvrouw, A. Mehta, The use of functionally graded poly-SiGe layers for MEMS applications, Funct. Grad. Mater. VIII 492–493 (2005) 255–260.
[14] Z. Lee, C. Ophus, L.M. Fischer, N. Nelson-Fitzpatrick, K.L. Westra, S. Evoy, Metallic NEMS components fabricated from nanocomposite Al–Mo films, Nanotechnology 17 (12) (2006) 3063–3070.
[15] D.C.C. Lam, F. Yang, A.C.M. Chong, J. Wang, P. Tong, Experiments and theory in strain gradient elasticity, J. Mech. Phys. Solids 51 (2003) 1477–1508.
[16] A.W. McFarland, J.S. Colton, Role of material microstructure in plate stiffness with relevance to microcantilever sensors, J. Micromech. Microeng. 15 (2005) 1060–1067.
[17] A.C.M. Chong, D.C.C. Lam, Strain gradient plasticity effect in indentation hardness of polymers, Mater. Res. 14 (10) (1999) 4103–4110.
[18] Kong. Shengli, Zhou. Shenjie, Nie. Zhifeng, Wang. Kai, The size-dependent natural frequency of Bernoulli-Euler micro-beams, Int. J. Eng. Sci. 46 (2008) 427–437.
[19] R.A. Toupin, Elastic materials with couple-stresses, Arch. Ration. Mech. Anal. 11 (1) (1962) 385–414.
[20] R.D. Mindlin, H.F. Tiersten, Effects of couple-stresses in linear elasticity, Arch. Ration Mech. Anal. 11 (1) (1962) 415–448.
[21] A.C. Eringen, Nonlocal polar elastic continua, Intl. J. Eng. Sci. 10 (1972) 1–16.
[22] AC. Eringen, Theory of micropolar plates, Zeitschrift fur angewandte Math. Phys. 18 (1967) 12–30.
[23] E.C. Aifantis, Strain gradient interpretation of size effects, Int. J. Fract. 95 (1999) 1–4.
[24] M.E. Gurtin, J. Weissmuller, F. Larche, The general theory of curved deformable interfaces in solids at equilibrium, Philos. Mag. A 178 (1998) 1093–1109.
[25] F. Yang, A.C.M. Chong, D.C.C. Lam, P. Tong, Couple stress based strain gradient theory for elasticity, Int. J. Solids Struct. 39 (10) (2002) 2731–2743.
[26] S.K. Park, X.L. Gao, Bernoulli-Euler beam model based on a modified couple stress theory, Micromech. Microeng. 16 (11) (2006) 2355–2359.
[27] H.M. Ma, X.L. Gao, J.N. Reddy, A microstructure-dependent Timoshenko beam model based on a modified couple stress theory, J. Mech. Phys. Solids 56 (2008) 3379–3391.
[28] A.C.M. Chong, F. Yang, D.C.C. Lam, P. Tong, Torsion and bending of micron-scaled structures, J. Mater. Res. 16 (2001) 1052–1058.
[29] D.V. Scheible, A. Erbe, R.H. Blick, Evidence of a nanomechanical resonator being driven into chaotic response via the Ruelle-Takens route, Appl. Phys. Lett. 81 (2002) 1884–1886.
[30] M. Simsek, J.N. Reddy, Bending and vibration of functionally graded micro beams using a new higher order beam theory and the modified couple stress theory, Int. J. Eng. Sci. 64 (2013) 37–53.
[31] M. Asghari, M.T. Ahmadian, M.H. Kahrobaiyan, M. Rahaeifard, On the sizedependent behavior of functionally graded micro beams, Mater. Des. 31 (2010) 2324–2329.
[32] M. Asghari, M. Rahaeifard, M.H. Kahrobaiyan, M.T. Ahmadian, The modified couple stress functionally graded Timoshenko beam formulation, Mater. Des. 32 (2011) 1435–1443.
[33] A. Arbind, J.N. Reddy, Nonlinear analysis of functionally graded microstructure-dependent beams, Comp. Struct. 98 (2013) 272–281.
[34] A. Arbind, J.N. Reddy, A.R. Srinivasa, Modified couple stress-based third-order theory for nonlinear analysis of functionally graded beams, Lat. Am. J. Solids Struct. 11 (2014) 459–487.
[35] J. Awrejcewicz, V.A. Krysko, I.V. Papkova, A.V. Krysko, Routes to chaos in continuous mechanical systems. Part 1: Mathematical models and solution methods, Chaos Solit. Frac. 45 (2012) 687–708.
[36] A.V. Krysko, J. Awrejcewicz, S.P. Pavlov, M.V. Zhigalov, V.A. Krysko, On the iterative methods of linearization, decrease of order and dimension of the Kármán-type PDEs, Sci. World J. (2014) 15 pages.
[37] V.F. Kirichenko, J. Awrejcewicz, A.F. Kirichenko, A.V. Krysko, V.A. Krysko, On the nonclassical mathematical models of coupled problems of thermo-elasticity for multi-layer shallow shells with initial imperfections, Int. J. NonLin. Mech. 74 (2015) 51–72.
[38] J. Awrejcewicz, A.V. Krysko, V. Soldatov, On the wavelet transform application to a study of chaotic vibrations of the infinite length flexible panels driven longitudinally, Int. J. Bif. Chaos 19 (10) (2009) 3347–3371.
[39] J. Awrejcewicz, A.V. Krysko, I. Kutepov, N. Zagniboroda, M. Zhigalov, V.A. Krysko, Analysis of chaotic vibrations of flexible plates using fast fourier transforms and wavelets, Int. J. Struc. Stab. Dyn. 13 (7) (2013) 1340005-1–1340004-12.
[40] J. Awrejcewicz, O.A. Saltykova, M.V. Zhigalov, P. Hagedorn, V.A. Krysko, Analysis of nonlinear vibrations of single-layered Euler-Bernoulli beams using wavelets, Int. J. Aero. Light. Struct. 1 (2) (2011) 203–219.
[41] A.V. Krysko, J. Awrejcewicz, M.V. Zhigalov, V.A. Krysko, On the contact interaction between two rectangular plates, Nonlin. Dyn. 85 (4) (2016) 2729–2748.
[42] A.V. Krysko, J. Awrejcewicz, O.A. Saltykova, M.V. Zhigalov, V.A. Krysko, Investigations of chaotic dynamics of multi-layer beams using taking into account rotational inertial effects, Comm. Nonlin. Sci. Num. Simul. 19 (8) (2014) 2568–2589.
[43] V.A. Krysko, J. Awrejcewicz, I.E. Kutepov, N.A. Zagniboroda, A.V. Serebryakov, A.V. Krysko, I.V. Papkova, Chaotic dynamics of flexible beams with piezoelectric and temperature phenomena, Phys. Lett. A 377 (2013) 2058–2061.
[44] J. Awrejcewicz, V.A. Krysko, I.E. Kutepov, N.A. Zagniboroda, V. Dobriyan, I.V. Papkova, A.V. Krysko, Chaotic vibrations of flexible curvilinear beams in temperature and electric fields, Int. J. NonLin. Mech. 76 (2015) 29–41.
[45] J. Awrejcewicz, A.V. Krysko, I.V. Papkova, V.M. Zakharov, N.P. Erofeev, E.Yu. Krylova, J. Mrozowski, V.A. Krysko, Chaotic dynamics of flexible beams driven by external white noise, Mech. Sys. Sig. Proc. 79 (2016) 225–253.

[46] J. Awrejcewicz, V.A. Krysko, I.V. Papkova, A.V. Krysko, Deterministic Chaos in One Dimensional Continuous System, World Scientific, Singapore, 2016.
[47] S.P. Timoshenko, On the correction for shear of differential equation for transverse vibration of prismatic bar, Philos. Mag. 41 (1921) 744–746.
[48] L.L. Ke, Y.S. Wang, J. Yang, S. Kitipornchai, Nonlinear free vibration of size-dependent functionally graded microbeams, Int. J. Eng. Sci. 50 (1) (2012) 256–267.
[49] A.V. Krysko, J. Awrejcewicz, I.E. Kutepov, N.A. Zagniboroda, V. Dobriyan, V.A. Krysko, Chaotic dynamics of flexible Euler-Bernoulli beams, Chaos 34 (4) (2014) 043130-1–043130-25.
[50] V.A. Krysko, J. Awrejcewicz, S.A. Komarov, Nonlinear deformations of spherical panels ssubjected to transversal load action, Comput. Meth. Appl. Mech. Eng. 194 (27–29) (2005) 3108–3126.
[51] J.N. Franklin, On Tikhonov's method for ill-posed problems, Math. Comput. 28 (128) (1974) 889–907.
[52] K. Miller, Least squares methods for ill-posed problems with a prescribed bound, SIAM J. Math. Anal. 1 (1) (1970) 52–74.
[53] D.L. Phillips, A technique for the numerical solution of certain integral equations of the first kind, J. Assoc. Comput. Mach. 9 (1) (1962) 84–97.
[54] A. Wolf, J.B. Swift, H.L. Swinney, J.A. Vastano, Determining Lyapunov exponents from a time series, Physica D 16 (1985) 285–317.
[55] M.T. Rosenstein, J.J. Collins, C.J.F. De Luca, Practical method for calculating largest Lyapunov exponents from small data sets, Physica D 65 (1993) 117–134.
[56] H. Kantz, A robust method to estimate the maximal Lyapunov exponents of a time series, Phys. Lett. A 185 (1994) 77–87.
[57] G. Benettin, L. Galgani, A. Giorgilli, J.M. Strelcyn, Lyapunov exponents for smooth dynamical systems and Hamiltonian systems; a method for computing all of them, part I: theory, Meccanica 15 (1980) 9–20.
[58] I. Shimada, T. Nagashima, A numerical approach to ergodic problem of dissipative dynamical systems, Prog. Theor. Phys. 61 (6) (1979) 1605–1616.
[59] A. Stefanski, Estimation of the largest Lyapunov exponent in systems with impacts, Chaos Solit. Fract. 11 (15) (2000) 2443–2451.
[60] J. Awrejcewicz, A.V. Krysko, V. Dobriayn, Papkova, I.V. Papkova, Krysko, V.A. Krysko, On the Lypunov exponents computation of coupled nonlinear Euler-Bernoulli bealms, in: Proceedings of the XIV International Conference on Civil, Structural and Environmental Engineering Computing, Sept. 3–6, 2013, Italy. – Cagliari, 2013, p. 20.
[61] J. Awrejcewicz, V.A. Krysko, Feigenbaum scenario exhibited by thin plate dynamics, Nonlin. Dyn. 24 (2001) 373–398.
[62] J. Awrejcewicz, A.V. Krysko, M.V. Zhigalov, O.A. Saltykova, V.A. Krysko, Chaotic vibrations in flexible multilayered Bernoulli-Euler and Timoshenko type beams, Latin Am. J. Solids Struct. 5 (4) (2008) 319–363.